Phase and Rheological Behavior of Novel Gemini-Type Surfactant Systems

Durga P. Acharya,[†] Hironobu Kunieda,*[,†] Yositaka Shiba,[†] and Ken-ichi Aratani[‡]

Graduate School of Environment and Information Sciences, Yokohama National University, Tokiwadai 79-7, Hodogaya-ku, Yokohama 240-8501, Japan, and Chukyo Yushi Co., Ltd, 2-1 Tomikawa-cho, Nakagawa-ku, Nagoya 454-0037, Japan

Received: July 18, 2003; In Final Form: November 19, 2003

A novel anionic gemini-type surfactant with no spacer group, disodium 2,3-didodecyl-1,2,3,4-butanetetracarboxylate (GS), was investigated for its phase behavior in water, water/decane, and water/cosurfactant systems in a wide range of compositions. At low surfactant concentration in the GS−water binary system, a micellar solution phase is formed which transforms to a hexagonal (H_1) phase, as in conventional ionic surfactant systems. At high GS concentration, however, the H_1 phase transforms to the rectangular-ribbon (R_1) liquid−crystal phase. Since the GS molecule has no spacer group, a small cross-sectional area of the headgroup and closely packed hydrophobic chain tend to increase the packing constraints of the lipophilic core with increasing surfactant concentration, thereby inducing the H_1-R_1 phase transition. In the presence of a normal hydrocarbon like decane, the H_1 phase is changed to a micellar cubic phase. On the other hand, the surfactant layer curvature becomes less positive upon addition of a lipophilic amphiphile because it is solubilized in the palisade layer of the aggregate. Addition of short poly(oxyethylene) chain nonionic surfactant (C_mEO_n, where m, n = 12, 3; 12, 4; and 16, 4) to the aqueous GS solution in a dilute region increases the viscosity by several orders and forms a transparent and viscoelastic micellar solution showing the rheological properties of typical wormlike micelles, with Maxwellian behavior in low oscillatory frequency. In the GS−$C_{12}EO_3$ and also in the GS−$C_{16}EO_4$ systems, the viscosity values are significantly higher than the reported values for dimeric surfactants of similar chain length.

Introduction

Gemini surfactants, which have more than two hydrophilic and hydrocarbon chains, have a very high potential for practical applications because of their excellent ability to lower surface tension of water and low Krafft temperatures. Besides, the critical micelle concentration is extremely low. Moreover, it is expected that their biocompatibility would be good compared with a conventional surfactant because their skin penetration may be low due to their high molecular weight. However, the main factor that has prevented the use of gemini surfactants in practical applications is their high costs.

Recently, a novel gemini surfactant, disodium 2,3-didodecyl-1,2,3,4-butanetetracarboxylate (GS), was synthesized by a simple reaction using cyclic olefins and dicarboxylic acids. The general chemical structure of the gemini surfactant is shown in Figure 1. Most of the gemini surfactants studied in the past have a spacer chain between two hydrophilic groups in the molecule, usually represented by $m-s-m$, where m and s are the carbon numbers in the alkyl chains and of the alkanediyl spacer. The spacer chain is known to have a strong influence on the physicochemical properties of gemini surfactants.[1] For example, a cationic gemini surfactant with a short spacer chain shows viscoelastic properties in solution.[2,3] The effects of the spacer chain length, headgroups, and main hydrophilic chain length of gemini surfactant on the solution and surface properties have been extensively studied.[4,5] To our knowledge, the gemini surfactant without a spacer chain has not been studied for its surface and solution properties.

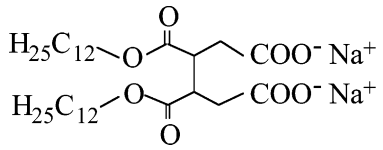

Figure 1. Molecular structure of GS.

Most of the studies on the phase behavior of the gemini surfactant solutions have been done in a dilute region[6−8] with only a few reports on the phase behavior of the gemini surfactant in a wide range of compositions.[9] Recently, it was found that an aqueous solution of a gemini surfactant having a spacer chain and carboxylate as headgroups forms a discrete cubic phase in the presence of hydrocarbon.[9] It would be interesting to know how the phase behavior of the gemini surfactant without a spacer chain differs from the behavior of one with spacer groups.

In this context, we have investigated the phase behavior of the novel dimeric surfactant, GS, in the presence of water, water/decane, and water/short poly(oxyethylene) nonionic surfactants in a wide range of compositions. We also studied the rheological behavior of highly viscous micellar solutions formed in a dilute region of the GS/nonionic mixed surfactant systems.

Experimental Section

Materials. A new gemini surfactant, GS, was synthesized in Chukyo Yushi Co., Japan. The chemical structure of the GS is shown in Figure 1. Decane (Tokyo Kasei Kogyo Co.), 1-decanol (Aldrich), and poly(oxyethylene)alkyl ether (abbreviated as C_mEO_n, with m, n = 12, 2; 12, 3; 12, 4; and 16, 4) (Nikko Chemicals Co.) were used as received.

* Author to whom correspondence may be addressed. Fax: +81-45-339 4190. E-mail: kunieda@ynu.ac.jp.
[†] Yokohama National University.
[‡] Chukyo Yushi Co., Ltd.

10.1021/jp036096b CCC: $27.50
Published on Web 01/13/2004

Synthesis of GS. *cis*-1,2,3,6-Tetrahydrophthalic anhydride (1 mol) was esterificated with 2 mol of 1-dodecanol in toluene in the presence of 0.01 mol of sulfuric acid as a catalyst. The product didodecyl-1,2,3,6-tetrahydrophthalate obtained was oxidized in the presence of potassium permanganate (1:2.7 molar ratio) in a mixed solvent of water and acetone at 10 °C for 3 h. The reaction mixture was acidified to pH ~ 1−2 by adding dilute sulfuric acid. The product 2,3-didodecyl-1,4-dihydrogen-1,2,3,4-butanetetracarboxylate thus obtained was extracted with diethyl ether and was recrystallized by a mixed solvent of ethyl acetate and hexane. GS was obtained by neutralizing 2,3-didodecyl-1,4-dihydrogen-1,2,3,4-butanetetracarboxylic acid with aq sodium hydroxide solution. To prevent hydrolysis, 2 mol % excess sodium hydroxide was added.

Phase Diagram. Required amounts of reagents were taken in glass ampules and sealed. The samples were homogenized at 50−70 °C using a vortex mixer and repeated centrifugation through narrow constriction. This mixing process was continued at least for 1−3 weeks. The samples were left in a water bath at 25 °C for more than a week for equilibration, and phases were identified by visual observation with the help of a cross polarizer. In the case of liquid crystals, polarizing microscopy and/or small-angle X-ray scattering (SAXS) was used to identify them.

SAXS. The interlayer spacing of the liquid crystals was measured by SAXS, performed on a small-angle-scattering goniometer with an 18-kW Rigaku Denki rotating anode goniometer (RINT-2500) at about 25 °C. The samples of the liquid crystals were lapped by plastic films for measurement (Myler seal method). The type of liquid crystals was determined from the ratio of the interlayer spacing corresponding to the peaks. For example, the SAXS peak ratios of the lamellar and (reverse) hexagonal phases are $1:{}^1/_2:{}^1/_3$ and $1:{}^1/_{\sqrt{3}}:{}^1/_2$..., respectively.

Rheological Measurements. Samples for the rheological measurements were prepared by adding the required amount of $C_{12}EO_n$ to the measured volume (5−10 mL) of an aqueous GS solution (5 wt %, ~0.081 M). The samples were homogenized and left in a water bath at 25 °C for at least 48 h to ensure equilibration before performing measurements. Rheological measurements were performed in an ARES rheometer (Rheometric Scientific) at 25 °C (unless otherwise stated) using couette (cup diameter, 34 mm; bob diameter, 32 mm; and bob length, 33.3 mm) and cone plate (two sizes: 50 and 25 mm diameter, each having a cone angle of 0.04 rad) geometries, depending on the viscosity of the sample. Dynamic frequency-sweep measurements were performed in the linear viscoelastic regime of the samples, as determined previously by dynamic strain sweep measurements.

Results and Discussion

Phase Behavior of Binary Water−GS System. The phase diagram of the water−GS system was constructed, and the result is shown in Figure 2. With the increasing surfactant concentration (plotted horizontally as wt % in the aqueous surfactant system), an aqueous micellar solution (W_m) phase is formed, and progressively, an H_1 phase composed of very long rodlike aggregates arranged in hexagonal array is produced. This behavior is similar to that observed for an amino acid based gemini surfactant of similar ionic group and comparable chain length but with a $-(CH_2CH_2)-$ spacer group,[9] although the W_m-H_1 transformation in the GS system takes place at a comparatively smaller surfactant concentration. At low temperatures, the H_1 phase is changed to isotropic viscous solution,

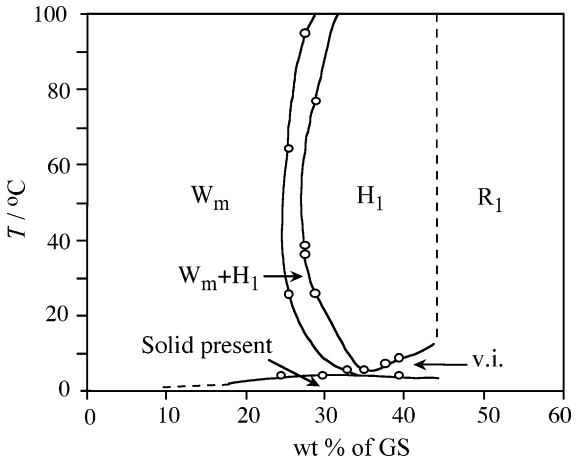

Figure 2. Partial phase diagram of GS−water binary system. W_m is the micellar phase; H_1 and R_1 are the hexagonal and the rectangular-ribbon liquid−crystal phases, respectively. v.i. is the unidentified viscous isotropic phase. The phase boundary between the solid and the R_1 phase has not been determined accurately and therefore has not been shown here.

as is shown in Figure 2. We have not studied the structure of this phase. At a high GS concentration region (above ~45 wt %), the H_1 phase transforms into a R_1 phase composed of very long rodlike aggregates with somewhat elliptical cross sections arranged in a rectangular lattice with primitive (*pgg*) or centered (*cmm*) symmetry.[10,11] The structure of the R_1 phase and its evolution from the H_1 phase with increasing surfactant concentration will be presented shortly later. The R_1 phase, one of the intermediate phases located between the H_1 and L_α phases in phase diagram, is formed as a result of the structural deformation of the circular cross section of the aggregate of the H_1 phase upon increasing the packing constraint in the incompressible lipophilic core, for example, by adding more surfactant[12] or a long-chain alcohol such as decanol.[13,14]

The H_1-R_1 phase transition in the GS system may be attributed to the absence of a spacer group or small interfacial area, a_s, and closely spaced hydrophobic chains, due to which the packing constraint in the lipophilic core increases on successive addition of the double-chain surfactant to the H_1 phase. As a result, the average interfacial curvature of the aggregate decreases, and the circular cross section of the rodlike aggregate gets deformed to an elongated shape. In the system of the dimeric surfactant with a spacer chain,[9] on the other hand, the presence of the spacer group makes the curved interface of aggregates, such as micellar aggregates or rodlike aggregates with circular cross sections, relatively more stable, as suggested by the W_m-H_1 phase transformation occurring at comparatively higher surfactant concentrations, as mentioned above, comparatively wider H_1 regions up to high surfactant concentration (~67 wt %), and also the H_1-L_α transformation taking place via the bicontinuous cubic (V_1) phase consisting of interconnected rodlike aggregates.

In the phase diagram (Figure 2), the approximate phase boundary between the H_1 and R_1 phases has been shown by a dotted line, and the region of the R_1 phase includes a single R_1 phase and multiphases containing the R_1 phase.

Structures of the R_1 Phase. The SAXS pattern of the R_1 phase has the first two very intense peaks, which are followed by weak peaks,[10,15] as is shown in Figure 3. The Bragg's reflections for the R_1 phase is given by the following equation[10]

$$d_{hk} = \left(\frac{h^2}{a^2} + \frac{k^2}{b^2}\right)^{-1/2} \quad (1)$$

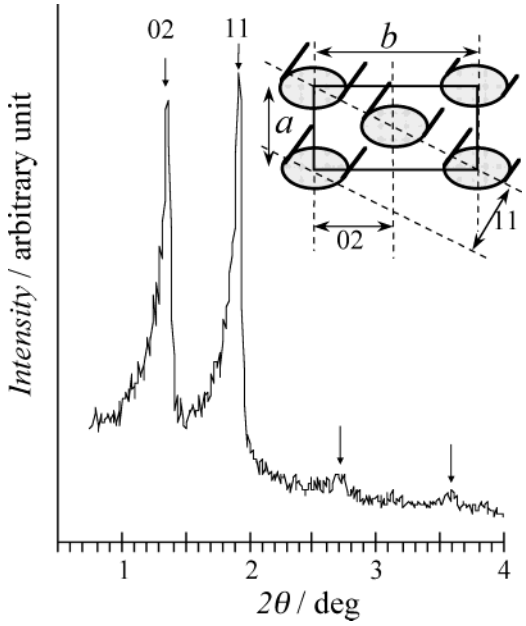

Figure 3. SAXS pattern of the R_1 phase of the GS−water system (48.1 wt % of GS) at 25 °C. The schematic structure of the R_1 phase of *cmm* symmetry with unit cell parameters *a* and *b* is also shown.

where *d* is the spacing corresponding to the reflection by the *hk* plane and *a* and *b* are the unit cell parameters, as shown in Figure 3. For *pgg* symmetry, Miller indices *h* and *k* can have any positive integer *n*, with the restrictions that for $h = 0$, $k = 2n$ and $k = 0$, $h = 2n$. For *cmm* symmetry, $h + k = 2n$, where $n \geq 0$. In the SAXS pattern shown in Figure 3, the positions of the available peaks—two intense peaks and two higher-order weak peaks indicated by arrows—fit to both the *cmm* and *pgg* structures, with the first two intense peaks assigned to the (02) and (11) planes, respectively. The unit cell dimensions of $a = 4.92$ nm and $b = 12.98$ nm can be obtained from eq 1. Absence of a d_{12} peak at $2\theta \sim 2.25°$, which is crucial in distinguishing *cmm* from *pgg* symmetry, suggests that the structure most probably has a *cmm* symmetry.

Figure 4 shows the evolution of the SAXS pattern of the liquid−crystal phases with increasing GS concentration. Up to 42.4% GS concentration, we can see the SAXS patterns typical of the H_1 phase, with continuously decreasing interlayer spacing with decreasing water concentration in the system. At 45% GS, a very weak band appears at a low angle (indicated by an arrow), which develops as an intense (02) peak of the R_1 phase on increasing GS concentration to 47.6%. In the present system, the R_1 region is rather wide in comparison with conventional surfactant systems. With increasing concentration of GS or decreasing water content, gradual shift of the (02) peak to a low angle (increase in *b*) suggests a progressive deformation or elongation of the cross section of the aggregates. Similarly, the shift of the (11) peak to a large angle (decrease in *a*) corresponds to the decrease in the separation between the aggregates. The decreasing intensity of the low-angle (02) peak and persistence of the intense (11) peak at a high GS concentration (57.4−60.0%) show that the rectangular symmetry is gradually broken, leading to the formation of a new structure, most probably a lamellar structure by lateral fusion of the ribbonlike aggregate in the (11) plane. We have recently studied the R_1-L_α phase transformation and shown an epitaxial relationship between the (11) plane of the R_1 phase and the (01) plane of the L_α phase in an ionic surfactant/decanol/water system.[15]

Phase Behavior of a Water/GS/Decane System. Figure 5 shows the phase behavior of a water/GS/decane system.

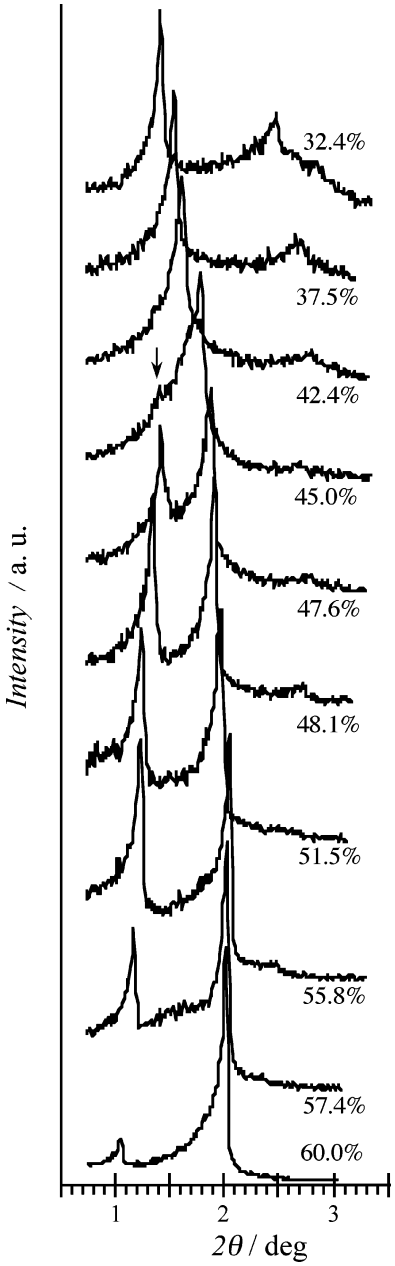

Figure 4. Evolution of the SAXS diffractograms of the mesophases with increasing surfactant concentration (wt % of GS) in the GS−water system.

Solubilazation of the hydrocarbon in the W_m phase is low, and beyond the solubilization limit, an excess oil phase is separated and the two-phase region is obtained. The solubilization of the hydrocarbon oil in the H_1 phase induces a H_1-I_1 (isotropic cubic phase) transition, as observed previously in the anionic gemini surfactant with a spacer chain.[9] It is well known that the H_1-I_1 phase transition of hydrophilic surfactant takes place upon addition of hydrocarbon. Since the hydrocarbon chain length of a surfactant molecule is limited and cannot exceed that of the extended form, a spherical micelle is not able to form if the effective cross-sectional area is not large enough for the packing constraint. However, if a hydrocarbon oil is solubilized in a rod micelle and makes an oil pool in the micellar core, the rod−sphere phase transition can occur.[16,17] Beyond the solubilization limit of the I_1 phase, an excess oil phase separates and the $I_1 + O$ two-phase region is observed. The phase boundary in the high surfactant concentration region of the I_1 phase could not

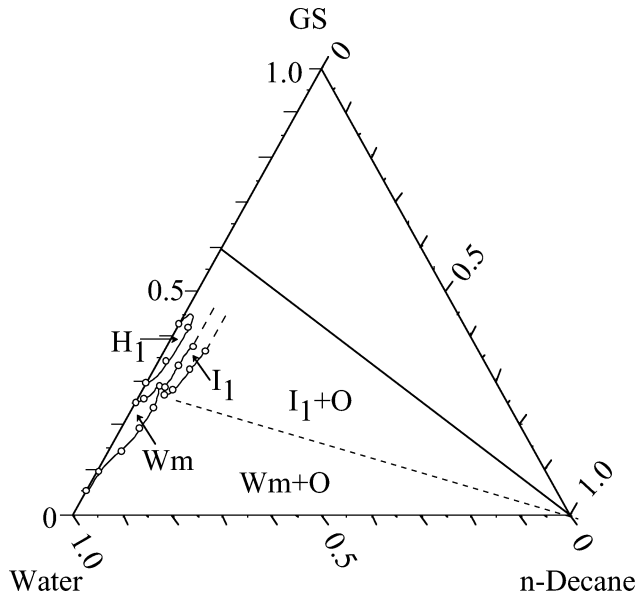

Figure 5. Phase diagram of the GS/water/decane system at 25 °C. I_1 and O are the isotropic cubic liquid−crystal and oil phases respectively; other notations are the same as Figure 4.

be ascertained due to the difficulty in the mixing process caused by very high viscosity of the samples in the region.

Phase Behavior of Water/GS/C_mEO_n Systems. Different from hydrocarbons, lipophilic amphiphiles tend to be solubilized in a surfactant palisade layer and reduce the surfactant layer curvature. Figure 6 shows the partial phase diagrams of water/GS/C_mEO_n systems in the dilute region. It can be seen from these figures that the width of the W_m phase, i.e., the ability of the W_m phase, to solubilize the nonionic amphiphile at low surfactant concentration increases with increasing number of EO units in $C_{12}EO_n$; and with $C_{12}EO_4$, the W_m phase protrudes toward the $C_{12}EO_4$ apex. It is known that at 25 °C, these nonionic amphiphiles cannot form a micellar phase in the water-rich region of water−surfactant binary systems; $C_{12}EO_3$ (up to ∼45 wt %) and $C_{12}EO_4$ (up to ∼25 wt %) form a two-phase region of lamellar (L_α) liquid crystals[18], and $C_{16}EO_4$ remains as a solid.[19] Incorporation of a small amount of ionic surfactant (GS) to the aggregate formed in the water−$C_{12}EO_4$ binary system induces a positive aggregate curvature to form micellar aggregates. With a decrease in the EO chain or an increase in the hydrocarbon chain length, however, the amphiphile becomes less hydrophilic, the ability of GS to induce the W_m phase is limited to a lower C_mEO_n content region, and, consequently,

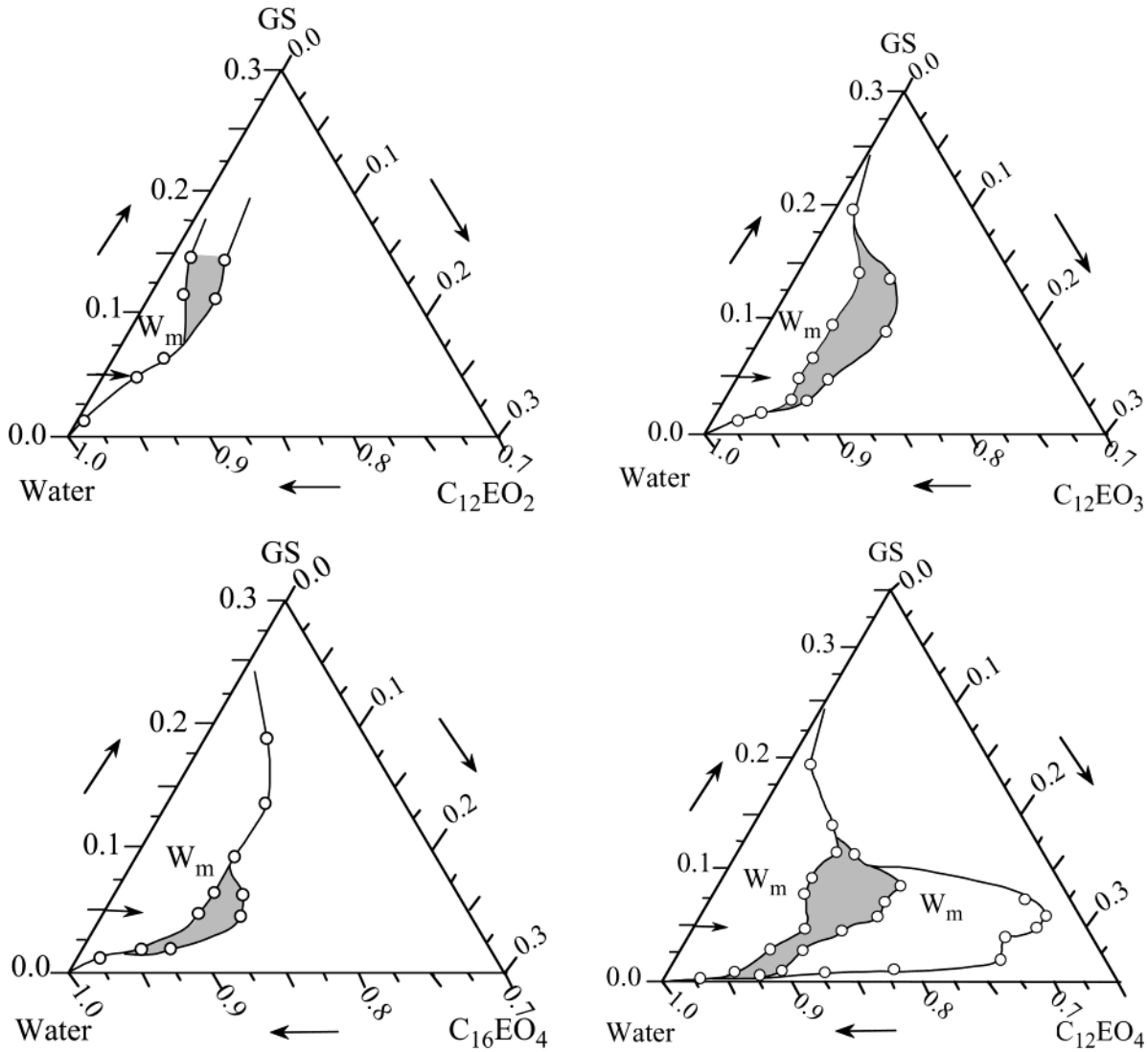

Figure 6. Partial phase diagrams of the water/GS/C_mEO_n systems at 25 °C. The high-viscosity region is shown by a shaded region inside the W_m region.

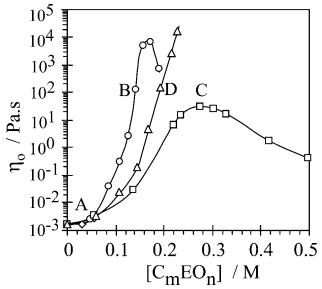

Figure 7. Variation of zero-shear viscosity (η_o) with C_mEO_n concentration in 5% GS−C_mEO_n systems at 25 °C. (A) $C_{12}EO_2$, (B) $C_{12}EO_3$, (C) $C_{12}EO_4$, (D) $C_{16}EO_4$.

the micellar region shrinks toward the lower C_mEO_n content in the ternary phase diagram, as is shown in Figure 6.

An interesting feature of these phase diagrams is that inside the W_m-phase region, there exists a region where the viscosity of the samples is unusually high. The viscous solutions are shear birefringent, that is, they become optically anisotropic when a sudden jerk is applied. The high-viscosity regions are extended nearly parallel to the GS−water binary axis and are shown approximately by the shaded area in the phase diagrams. In all the systems except GS−$C_{12}EO_4$, the viscous micellar solution is observed near the boundary of the W_m phase. The effect of the size of hydrophilic and lipophilic groups of the nonionic amphiphiles on the rheological behavior is discussed in the following section.

Rheological Behavior. Figure 7 shows the variation of zero-shear viscosity (η_o) with the increasing concentration of $C_{12}EO_n$ in 5 wt % (∼0.081 M) GS−$C_{12}EO_2$, −$C_{12}EO_3$, −$C_{12}EO_4$, and −$C_{16}EO_4$ systems within the W_m-phase region, as shown by the arrows in the corresponding phase diagrams (Figure 6). In the GS−$C_{12}EO_2$ system, the W_m-phase region is narrow and phase separation occurs before any noticeable increase in viscosity is observed whereas a sharp increase in η_o of the order of 6 is observed in GS−$C_{12}EO_3$ systems, and the viscosity reaches to ∼7500 Pa s, followed by a decrease. This viscosity value is noticeably higher (by 1 order) than the value reported for a dimeric surfactant with similar chain length.[2,4] With the further addition of the nonionic amphiphile, phase separation occurs. However, in the GS−$C_{12}EO_4$ system, the increase in η_o is less rapid, with the maximum value of ∼25 Pa s, and the viscosity peak is observed at a higher mixing fraction of the nonionic cosurfactant. In the GS−$C_{16}EO_4$ system, the viscosity attains a very high value (∼17 000 Pa s). However, a phase separation occurs before a viscosity maxima is observed. The η_o composition curves of the GS−$C_{12}EO_4$ and GS−$C_{16}EO_4$ systems (Figure 7) show that the latter system has a higher viscosity at similar concentrations of the nonionic amphiphile. The figure suggests that increasing the EO chain length (or n) and length of lipophilic chain length (or m) of C_mEO_n in the mixed aggregate affects the viscosity in the opposite way, increasing n tends to decrease η_o whereas increasing m would increase it.

In the GS−$C_{12}EO_3$, −$C_{12}EO_4$, and −$C_{16}EO_4$ systems, the viscoelastic micellar solutions are formed at compositions around the maximum-viscosity region. The viscoelasticity of the micellar solution is attributed to the entanglement of very long and flexible aggregates, often called "wormlike micelles", to form a transient network. Oscillatory shear rheology of the viscoelastic micellar systems at low shear frequency (ω) generally follows Maxwell fluid behavior with a single stress relaxation time (τ_R),[20] and the elastic modulus G' and the viscous modulus G'' are related to the shear frequency, ω, by following relations

$$G' = \frac{(\omega\tau_R)^2}{1 + (\omega\tau_R)^2} G_0 \tag{2}$$

$$G'' = \frac{\omega\tau_R}{1 + (\omega\tau_R)^2} G_0 \tag{3}$$

The relaxation time, τ_R, can be estimated as ω_C^{-1}, where ω_C is the frequency at which two moduli are equal. At high ω, the G' attains a limiting value called a plateau modulus, G_o. In surfactant systems where the G' does not give a constant limiting value, the G_o may be estimated from the modulus value at ω_R, using the relation $G_o = 2G''_{max}$, where G''_{max} is the viscosity modulus at the shear frequency ω_C. The zero-shear viscosity (η_o) is given by the relation[21]

$$\eta_o = G_o\tau_R \tag{4}$$

The complex viscosity, η^*, is related to the storage and loss moduli and η_O by the relations

$$\frac{(G'^2 + G''^2)^{1/2}}{\omega} = |\eta^*| = \frac{\eta_O}{(1 + \omega^2\tau_R^2)^{1/2}} \tag{5}$$

From eq 5, it follows that η_o can be estimated by extrapolating the $|\eta^*|$ to $\omega = 0$.

The living polymer model proposed by Cates et al.[22] describes the dynamics of the viscoelastic micellar system by combining the reptation model of polymer dynamics with the effect of reversible scission on viscoelastic properties. The model involves two time scales of stress relaxation, namely, reptation time (τ_{rep}), which corresponds to the curvilinear diffusion of a chain of the mean length along its own contour, and breaking time (τ_b). When breaking occurs often over the time scale of reptation ($\tau_{rep} \gg \tau_b$), as in a typical wormlike micellar system, the chain undergoes many breakages and recombinations before a chain segment relaxes by reptation, the stress relaxation is characterized by a new time scale given by $\tau_R = (\tau_b\tau_{rep})^{1/2}$, and the solution behaves as a Maxwell fluid with single relaxation time, τ_R.

Figures 8, 9, and 10 show the results of oscillatory shear measurements of the viscoelastic solutions of the GS−C_mEO_n systems in the vicinity of the maximum-viscosity region of the η_o composition curves shown in Figure 7. The evolution of viscoelastic properties of the GS−$C_{12}EO_3$ system with increasing concentration of the nonionic amphiphile is shown is Figure 8a. It can be seen that the systems show liquidlike behavior ($G'' > G'$) at low ω values and solidlike behavior ($G' > G''$) at high ω values. These rheological patterns are typical of viscoelastic wormlike micellar solutions with Maxwellian fluid behavior. Figure 8b shows Cole−Cole plots,[23] i.e., the plots of G'' against G', for the viscoelastic GS−$C_{12}EO_3$ systems shown in Figure 8a. In this plot, a Maxwell material is characterized by a semicircle with a diameter equal to G_o, or more correctly, the lower limit of G_o, as wormlike micellar systems often deviate from Maxwellian behavior at high ω. It can be seen from Figure 8b that, at lower concentrations of $C_{12}EO_3$, the system shows Maxwellian behavior in a wide range of frequencies, that is, $\tau_R \gg \tau_b$ is followed and stress relaxation occurs by reptation.

For wormlike micellar solution with the Maxwellian behavior, such as the GS−$C_{12}EO_3$ system at 0.173 M $C_{12}EO_3$ (parts a and b of Figure 8), the ratio of entanglement length (l_e) to the

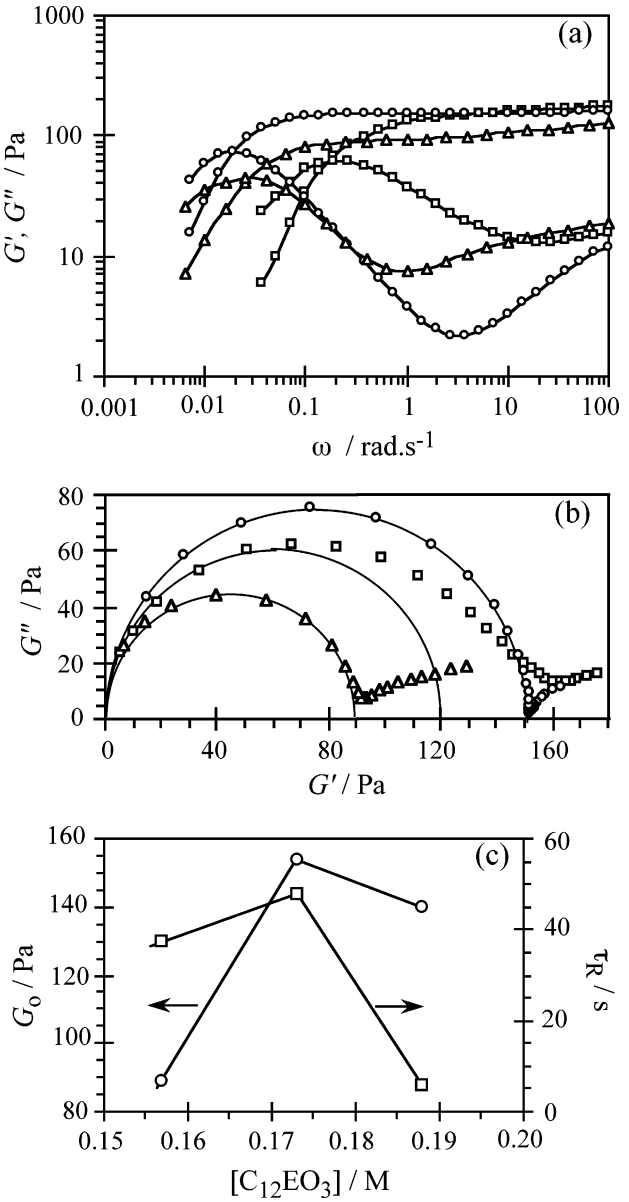

Figure 8. Variation of the storage modulus (G', open symbols) and loss modulus (G'', filled symbols) with oscillatory shear frequency (ω) for viscoelastic solutions of 5% GS−$C_{12}EO_3$ systems at different concentrations of $C_{12}EO_3$ (0.157 M (triangles), 0.173 M (circles), and 0.188 M (rectangles) (a), and corresponding Cole−Cole plot (b). The plateau modulus (G_o) and relaxation time (τ_R) for each of these systems are plotted with corresponding $C_{12}EO_3$ concentration (c).

micellar contour length (L) is related to the ratio of the minimum at G'' at high-frequency region (G''_{min}) and G_o by the relation[22]

$$\frac{G''_{min}}{G_o} \approx \frac{l_e}{L} \tag{6}$$

For this system, l_e, which is the average length between two entanglement points, is not currently available. Therefore, we cannot estimate the value of the micellar contour length, L. However, the ratio G''_{min}/G_o is about 0.014, which is, in our knowledge, the lowest value reported for wormlike micelles. The lowest value reported so far is 0.016 for a cationic surfactant with a long unsaturated tail.[24] For a typical value of l_e (80−150 nm) for wormlike micelles, the L corresponds to roughly 6−11 μm for the wormlike micelles of the GS−$C_{12}EO_3$ system. Another piece of information that can be obtained from the G''_{min} is the average scission time for the micelle, τ_b, which is approximately equal to the inverse of ω corresponding to the minimum of G''_{min} in the high-frequency region. For the GS−$C_{12}EO_3$ system at 0.173 M $C_{12}EO_3$, the estimated value of τ_b is ∼0.35 s. This value also allows us to estimate $\tau_{rep} \sim 6500$ s, using the $\tau_R = 47.6$ s obtained from oscillatory shear measurement. The estimated τ_{rep}, as well as experimental τ_R, indicates the presence of very long micelles.

With the further increase in $C_{12}EO_3$ concentration ([$C_{12}EO_3$] ∼ 0.19 M), the system comes near to the W_m phase boundary and noticeable deviation from the Maxwellian behavior is observed in the high-frequency region, suggesting a wide spectrum of fast stress relaxation processes.

Variation of G_o and τ with the concentration of $C_{12}EO_3$ in the system is shown in Figure 8c. Upon an increase in $C_{12}EO_3$ concentration from 0.157 to 0.173 M, G_o increases by nearly 70% and τ increases by ∼27%. Since G_o depends on the number density of the aggregates and τ can be associated with the length of the aggregate for the wormlike micellar system undergoing stress relaxation by reptation, as indicated by the Maxwellian behavior (see Figure 8b) for these systems, increase in these quantities may be associated with the micellar growth leading to longer micelles and increased number of entanglements that make the system more viscoelastic. With further increase in $C_{12}EO_3$ concentration to 0.188 M, however, G_o decreases slightly (by ∼7%, considering G_o to be equal to the diameter of the semicircle of the Cole−Cole plot) while a sharp decrease in τ (by about 9 times), and, consequently, in η_o (shown in Figure 7) is observed, which suggests a structural change leading to the formation of a micellar system with a nearly similar network structure but allows stress relaxation by additional faster mechanism. A plausible explanation for this observation is that the wormlike micelles get connected with each other, forming joints that can slip along their length, thereby allowing a faster and easier way of stress relaxation.[25] In a number of surfactant systems,[26,27] including a 12-2-12 gemini surfactant system,[4] such micellar connections or branching points have been detected by cryogenic transmission electron microscopy, especially in the region where the viscosity decreases after a maximum as a function of increasing concentration of surfactant or counterion.

In GS−$C_{12}EO_4$ systems, G'−G'' crossover occurs in the high-frequency region (Figure 9), which corresponds to a fast relaxation process. No data points are available at $\omega > 100$ rad s^{-1}, and therefore, only limited information on stress relaxation above ω_c is available. However, judging from the Maxwellian behavior observed in a wide range of frequencies in the system at the maximum-viscosity region ([$C_{12}EO_4$] ∼ 0.28 M), as suggested by the Cole−Cole plot (Figure 9b), reptation is a predominant mechanism of stress relaxation at these compositions. Relatively fast stress relaxation observed in this system in comparison with the GS−$C_{12}EO_3$ system at the maximum-viscosity region may be taken as an indication of the presence of shorter wormlike micelles in the GS−$C_{12}EO_4$ system. This is not surprising because increasing the number of EO units of the headgroup of nonionic amphiphile in the mixed micelle is likely to increase the interfacial curvature of the aggregate or, in other words, decrease the average a_s of the amphiphiles in the aggregates less rapidly and stabilize the curved interface, such as end caps of the rodlike aggregates. Consequently, unidimensional growth is less favorable and viscosity maximum occurs at comparatively higher mixing fractions of the nonionic amphiphile. The effect of the a_s on the micellar growth explains qualitatively why the high-viscosity W_m region in the phase diagrams of the water/GS/C_mEO_n systems (Figure 6) is more

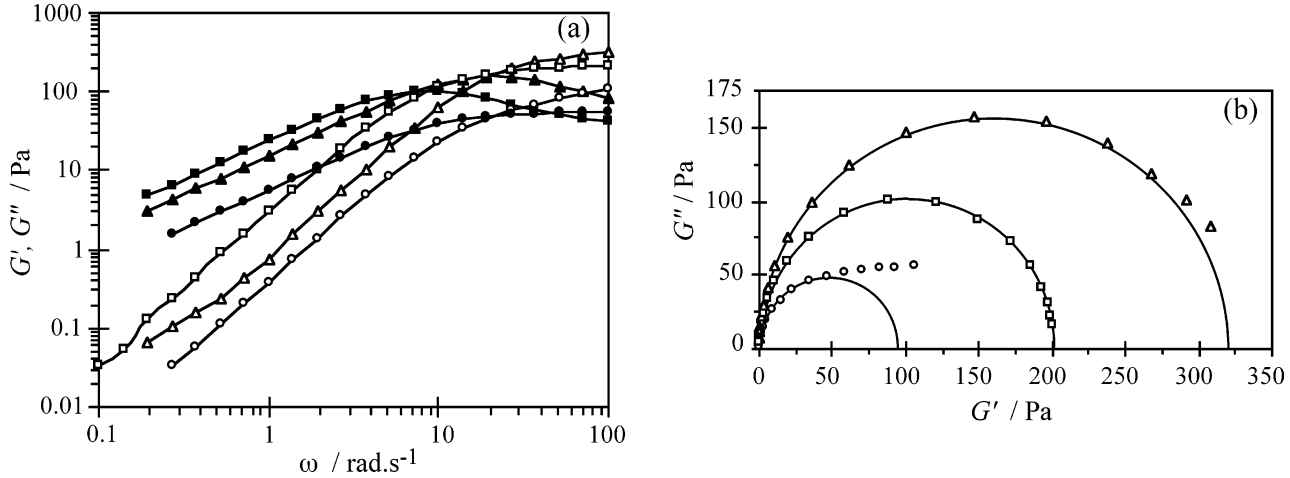

Figure 9. Variation of G' (open symbols) and G'' (filled symbols) with ω for the viscoelastic solutions of the 5% GS−$C_{12}EO_4$ systems at different concentrations of $C_{12}EO_4$, 0.220 M (circles), 0.276 M (rectangles), and 0.328 M (triangles) (a), and corresponding Cole−Cole plot (b)

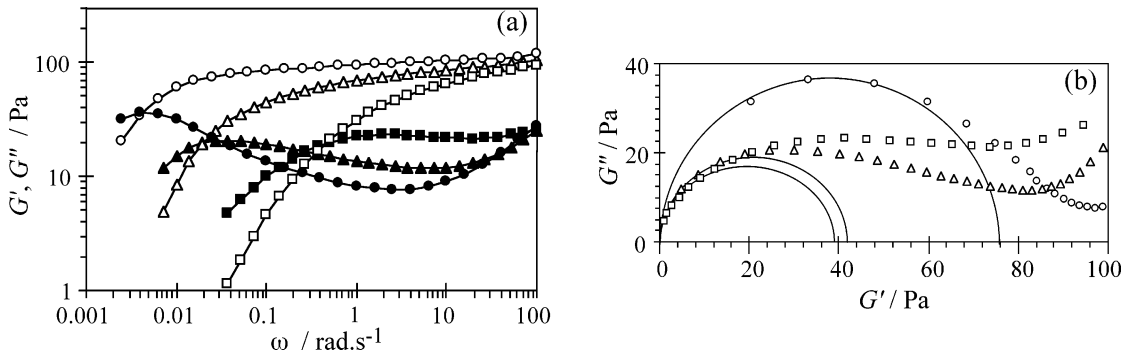

Figure 10. Variation of G' (open symbols) and G'' (filled symbols) with ω for viscoelastic solutions of 5% GS−$C_{16}EO_4$ systems at different concentrations of $C_{16}EO_4$, 0.191 M (rectangles), 0.215 M (triangles) and 0.227 M (circles) (a), and corresponding Cole−Cole plot (b).

or less parallel to the surfactant−water binary axis, i.e., the GS/C_mEO_n ratio required to form high-viscosity solution decreases with increasing GS concentration. With increasing surfactant (GS) concentration, a_s decreases even in a water−surfactant system. Hence, with increasing GS concentration and decreasing a_s, the mixing fraction of C_mEO_n for the rapid micellar growth (or viscosity) decreases, as is shown in Figure 6. Similar effect of the EO chain length and surfactant concentrations on rheological behavior has been observed in viscoelastic solutions of wormlike micelles formed in mixed nonionic systems of polyoxyethylene cholestryl ether and $C_{12}EO_n$ ($n = 1-4$)[28] and also in the mixed systems of CTAB and $C_{12}EO_n$.[29]

With the further increase in $C_{12}EO_4$ concentration, a noticeable deviation from Maxwellian behavior occurs at the high-frequency region, indicating the presence of an additional mechanism of stress relaxation, most probably the formation of the interconnected wormlike micelles, as mentioned previously. With the successive increase in the $C_{12}EO_4$ concentration, the samples become liquidlike ($G'' > G'$) in the experimental range of ω, and therefore, information on relaxation behavior could not be obtained. However, from Figure 7, it can be seen that η_o does not decrease sharply; rather, it decreases gradually, which may be taken as an indication that the network structure does not break abruptly.

In GS−$C_{16}EO_4$ systems, viscoelasticity increases with increasing concentration of the nonionic amphiphile (Figure 10), and the system gradually moves toward the Maxwellian behavior, as is shown by the corresponding Cole−Cole plot (Figure 10b). In the GS−$C_{16}EO_4$ system, phase separation occurs before the system exhibits a viscosity peak. However, it can be seen that in comparison to the GS−$C_{12}EO_4$ systems, the GS−$C_{16}EO_4$ systems have much lower crossover frequency at comparable surfactant concentration, which corresponds to the presence of very long wormlike micelles. This enhanced micellar growth observed by increasing the hydrocarbon chain length of the nonionic amphiphile, i.e., by substituting $C_{12}EO_4$ by $C_{16}EO_4$, may be associated with the ability of the longer hydrophobic chain to cause the packing constraint in the incompressible lipophilic core of the aggregate that would induce a sphere−rod transition if the aggregates are spherical or the formation of cylindrical (less curved) interface is favored over the highly curved (hemispherical) interface if the aggregates are already rodlike. Hence, this result is consistent with the relationship between the micellar growth and the ability of the C_mEO_n to reduce the interfacial curvature of the aggregate in the GS−C_mEO_n system.

Summary

A novel anionic gemini surfactant without a spacer group has been studied for its phase behavior in water, water/oil, and water/nonionic surfactant (C_mEO_n) systems in wide range of compositions. The GS−water binary system shows a phase behavior typical of ionic surfactant systems, a micellar solution phase and H_1 and R_1 liquid−crystal phases are formed successively with increasing surfactant concentration. Upon the addition of a hydrocarbon like decane, the H_1 phase is changed to a micellar cubic (I_1) phase. Addition of short poly(oxyethylene) chain nonionic surfactant ($C_{12}EO_3$, $C_{12}EO_4$, and $C_{16}EO_4$) to the aqueous GS solution in a dilute region expands the W_m-phase region and dramatically increases the viscosity by several orders and forms a transparent and viscoelastic micellar solutions

showing the rheological behavior typical of wormlike micellar solution. The viscoelastic behavior of the wormlike micellar solution in the maximum-viscosity region can be described by the Maxwell model at low shear frequency. Upon a decrease in the EO chain length or an increase in the lipophilic chain, the micellar growth is favored and the high-viscosity region is formed at lower mixing fraction C_mEO_n. D.P.A. thanks Kathmandu University, Nepal, for providing study leave.

References and Notes

(1) Zana, R. *J. Colloid Interface Sci.* **2002**, *248*, 203−220 and references therein.
(2) Kern, F.; Lequeux, F.; Zana, R.; Candau, S. J. *Langmuir* **1994**, *10*, 1714−1723.
(3) Oda, R.; Huc, I.; Homo, J.-C.; Heinrich, B.; Schmutz, M.; Candau, S. *Langmuir* **1999**, *15*, 2384−2390.
(4) Zana, R. *Adv. Colloid Interface Sci.* **2002**, *97*, 205−253.
(5) Tsubone, K.; Arakawa, Y.; Rosen, M. J. *J. Colloid Interface Sci.* **2003**, *262*, 516−524.
(6) Buhler, E.; Mendes, E.; Boltenhagen, P.; Munch, J. P.; Zana, R.; Candau, S. J. *Langmuir* **1997**, *13*, 3096−3102.
(7) Dreja, M.; Tieke, B. *Langmuir* **1998**, *14*, 800−807.
(8) Dreja, M.; Pyckhout-Hintzen, W.; Mays, H.; Tieke, B. *Langmuir* **1999**, *15*, 391−399.
(9) Kunieda, H.; Masuda, N.; Tsubone, K. *Langmuir* **2000**, *16*, 6438−6444.
(10) Gustafsson, S.; Quist, P.-O. *J. Colloid Interface Sci*. **1996**, *180*, 564−573.
(11) Hagslatt, H.; Soderman, O.; Jonsson, B. *Liq. Cryst.* **1992**, *12*, 667−688.
(12) Holmes, M. C. *Curr. Opinion Colloid Interface Sci.* **1998**, *3*, 485−492 and references therein.
(13) Acharya, D. P.; Lopez-Quintela, A. M.; Kunieda, H.; Oshimura, E.; Sakamoto, K. *J. Oleo Sci.* **2003**, *52*, 407−420.
(14) Hendrikx, Y.; Charvolin, J. *J. Phys.* **1981**, *42*, 1427−1440.
(15) Acharya, D. P.; Kunieda, H.; Oshimura, E.; Sakamoto, K. *Prog. Colloid Polym. Sci.*, accepted for publication.
(16) Kunieda, H.; Ozawa, K.; Huang, K.-L. *J. Phys. Chem. B* **1998**, *102*, 831−838.
(17) Kunieda, H.; Umizu, G.; Aramaki, K. *J. Phys. Chem. B* **2000**, *104*, 2005−2011.
(18) Huang, K.-L.; Sigeta, K.; Kunieda, H. *Prog. Colloid Polym. Sci.* **1998**, *110*, 171−174.
(19) Mitchell, D. J.; Tiddy, G. J. T.; Waring, L.; Bostock, T.; McDonald, M. P. *J. Chem. Soc., Faraday Trans. 1* **1983**, *79*, 975−1000.
(20) Rehage, H.; Hoffmann, H. *Molecular Phys.* **1991**, *74*, 933−973.
(21) Koehler, R. D.; Raghavan, S. R.; Kaler, E. W. *J. Phys. Chem. B* **2000**, *104*, 11035−11044.
(22) Granek, R.; Cates, M. E. *J. Chem. Phys.* **1992**, *96*, 4758−4767 and references therein.
(23) Hassan, P. A.; Candau, S. J.; Kern, F.; Manohar, C. *Langmuir* **1998**, *14*, 6025−6029.
(24) Raghavan, S. R.; Kaler, E. *Langmuir* **2001**, *17*, 300−306.
(25) Khatory, A.; Kern, F.; Lequeux, F.; Appell, J.; Porte, G.; Morie, N.; Ott A.; Urbach, W. *Langmuir* **1993**, *9*, 933−939.
(26) Lin, Z. *Langmuir* **1996**, *12*, 1729−1737.
(27) Danino D.; Talmon, Y.; Levy, H.; Beinert, G.; Zana, R. *Science* **1995**, *269*, 1420−1421.
(28) Acharya, D. P.; Kunieda, H. *J. Phys. Chem. B* **2003**, *107*, 10168−10175.
(29) Rodriguez, C.; Acharya, D. P.; Maestro, A.; Hattori, K.; Kunieda, H. *J. Chem. Eng. Japan*, in communication.